Journal of Physics:
Complexity

Conditions for skilful spatial and temporal tipping point early warning signals

Journal of Physics: Complexity

OPEN ACCESS

RECEIVED
31 December 2025

REVISED
4 March 2026

ACCEPTED FOR PUBLICATION
20 April 2026

PUBLISHED
7 May 2026

PAPER

Conditions for skilful spatial and temporal tipping point early warning signals

Joseph Clarke[1,2,*], **Chris Huntingford**[3], **Paul D L Ritchie**[1,2] **and Peter Cox**[1,2]

[1] Department of Mathematics and Statistics, Faculty of Environment, Science and Economy, University of Exeter, Exeter, Devon EX4 4QF, United Kingdom
[2] Global Systems Institute, University of Exeter, Devon, Exeter EX4 4QE, United Kingdom
[3] UK Centre for Ecology and Hydrology, Wallingford, Oxfordshire OX10 8BB, United Kingdom
[*] Author to whom any correspondence should be addressed.

E-mail: j.j.clarke@exeter.ac.uk

Keywords: tipping points, early warning indicators, climate change, resilience, dynamical systems

Abstract

As tipping points are extremely difficult to predict using an initial value modelling approach, forewarning of bifurcation tipping points instead often depends on the analysis of observational data, using approaches that aim to detect reducing system resilience. The most commonly used early warning indicators (EWIs) rely on the phenomenon of critical slowing down, which is the tendency for fluctuations of a state variable to get larger (increased variance) and longer lived (increased temporal autocorrelation), as the bifurcation is approached. This is measurable in low dimensional systems that remain close to a quasi-equilibrium state in the run-up to the bifurcation. However, in systems that are subject to rapid changes in external forcing, such as the contemporary Earth system, this condition is unlikely to be met and EWIs become less reliable. In addition, temporal EWIs require long observational time series. For these reasons, it makes sense to consider spatial EWIs that can make use of the spatial detail resolved by present-day observations, especially from remote sensing. In this paper, we explore the conditions under which spatial and temporal EWIs will each be reliable, using a simple spatially coupled model with a fold bifurcation. In the weak coupling limit, we find spatial EWIs give reliable warning of the bifurcation, even if the external forcing is changing rapidly. However, in the limit of strong spatial coupling, spatial early warning disappears. Under these conditions, we find temporal EWIs give reliable warning as long as the external forcing is not changing quickly compared to the characteristic timescale of the system. We conclude that spatial early warnings will be especially useful in systems that have relatively weak spatial coupling, but which are also subject to rapidly changing external forcing (e.g. forests under contemporary climate change).

1. Introduction

There is growing evidence that certain components of the Earth System, known as tipping elements [1], are bistable and that rising global temperatures may push these systems from one state to another [2, 3]. For example, the shutdown of the Atlantic meridional overturning circulation (AMOC) [4–6], the dieback of the Amazon Rainforest [7, 8] and the melting of ice sheets [9, 10] are all hypothesised tipping points that may be triggered by anthropogenic climate change.

Such transitions may lead to serious impacts. For example, the melting of the ice sheets could lead to multi-metre sea level rise [11]. A shutdown of the AMOC could cause decreases in temperature and precipitation across much of the northern hemisphere [12], with severe consequences for agriculture [13]. Furthermore, Amazon dieback could lead to cultural and biodiversity losses [14] as well as increased atmospheric CO_2 [7] as the Amazon is a significant store of carbon [15].

Modelling tipping points with earth system models (ESMs) has proven challenging and there is a large uncertainty in the magnitude of global temperature increase required to cause tipping [16]. Several

Table 1. Estimates of ϵ, which is the ratio of system to forcing timescale, for a subset of tipping elements using the estimated timescales in [16]. The forcing timescale was chosen to be 50 years. Assuming a current level of warming of around 1 K, if temperatures increase by 1 K over the forcing timescale then this choice of timescale corresponds to around 3 K of warming by the end of the century. This is about the level of warming expected under current policies [40].

Tipping element	System timescale (years)	Estimated ϵ
Greenland Ice Sheet	1000–15 000	20–300
West Antarctic Ice Sheet	500–13 000	10–260
Boreal Permafrost	10–300	0.2–6
AMOC	15–300	0.3–6
Amazon Rainforest	50–200	1–4
Southern Polar Gyre Convection	5–50	0.1–1

factors contribute to this uncertainty. For example, modelling some tipping points can involve very long simulations of inherently nonlinear systems across a range of parameter values [17]. This can prove computationally infeasible, particularly in the case of a fully coupled ESM. Furthermore, the equations governing biosphere dynamics are poorly defined. Therefore, different modelling approaches may disagree on the threshold or if tipping is actually possible [18]. Even in cases where the system is governed by Equations derivable from physical laws, such as the AMOC, ESMs still suffer biases in processes relevant to tipping [19]. In complex systems, tipping may not occur at a single critical threshold but instead proceed through a series of intermediate tipping points [20].

To help reduce this uncertainty, there have been attempts to determine empirically if a system is approaching a tipping point. If the tipping can be characterised as a bifurcation (i.e. it is an example of B-tipping [21]) then this is possible in principle. Methods designed to detect an approaching bifurcation typically make use of an assumption that the tipping element can be modelled as a dynamical system, subject to noise, that is near an equilibrium with slowly varying parameters. Mathematically, a bifurcation occurs when an eigenvalue of the Jacobian of the system's equation of motion, evaluated at equilibrium, crosses the imaginary axis [22]. As the Jacobian controls the linearised dynamics of the system, and the real part of its eigenvalues control the rate of relaxation to equilibrium, this change in the eigenvalues manifests as an increase in magnitude and duration of the fluctuations about the equilibrium of the system.

This loss of resilience is known as *critical slowing down*. It can be quantified by determining changes in the autocorrelation and variance, known as early warning indicators (EWIs), of a detrended time series. Their changes can be measured to give early warning signals (EWSs) of tipping [23]. As the tipping point is approached, the variance diverges and the autocorrelation tends to unity [24–26].

These techniques have been applied to Earth System tipping elements [27–32]. However, questions remain about how best to interpret these results in light of measurement uncertainties [33, 34], the addition of non-stationary processes [35] and applicability to high dimensional systems [36].

A basic assumption this approach makes is that there is a timescale separation between the forcing and the dynamics of the system [37]. In other words, the ratio of the timescale of the system response to the timescale of the forcing, ϵ, must be small [38]. If this assumption is met, then the system is always near a quasi-equilibrium and the fluctuations about that equilibrium can be related to the stability of the system. Furthermore, the slow forcing enables enough data about the fluctuations to be collected to give reliable statistics. Conversely, if this assumption does not hold, then it is difficult to detect critical slowing down [39].

This poses a particular challenge when trying to detect early warning signals from tipping elements forced by contemporary climate change, as this timescale separation cannot be guaranteed. This is because the decadal timescale of climate change is similar to, or faster than, the inherent timescales of some tipping elements. This is illustrated in table 1, which provides crude estimates of ϵ for different tipping elements.

Therefore it is important to adapt EWIs to work in rapidly forced systems. One method, examined in this work, is to use spatial EWIs. Intuitively, we may expect spatial EWIs to be more skilful than temporal early warning indicators in rapidly forced systems as they give an instantaneous snapshot of the system, whereas temporal EWIs give an average of the system's stability over a window.

There are a number of possible spatial EWIs. For example, Kéfi *et al* [41] found increased spectral power at long wave lengths, rising variability and changes to patchiness were all spatial indicators of an upcoming transition. Donangelo *et al* [42] compared spatial and temporal EWIs, finding that the

spatial variance can give an earlier early warning than the temporal variance. Spatial indicators have been investigated in ecological contexts [43–45] and have been applied to observational datasets [46–48].

One way to understand spatial EWIs is to consider how EWIs are created. An EWI can be derived by finding a quantity, defined as an ensemble average of a function of the system state, which has a characteristic behaviour as the tipping point is approached. Often these ensemble averages are estimated as averages of a time series, giving temporal EWIs. They can also be estimated by taking averages of a system over space. This space-for-time substitution can be justified if different points in space can be treated as different ensemble members.

A problem with this substitution is that it ignores the inevitable correlations between different points in space. If the system is un- or very weakly spatially coupled, these correlations will be unimportant and we may expect good EWSs. However, as the strength of spatial coupling increases, different points in space will be more strongly correlated and so we should expect spatial early warning signals to be worse.

In this paper we look at the effect of spatial coupling and forcing timescales on the skill of EWSs. We will compare the classical temporal EWIs with their space-for-time substitution equivalents. We use these particular spatial early warning indicators as they are simple and enable a natural comparison with their corresponding temporal indicators.

2. Methods

2.1. Model system

2.1.1. Without spatial interactions

We begin by considering a system without any spatial dependence and study the prospect of obtaining EWSs. To keep things as simple as possible, we take a one dimensional system with a saddle node bifurcation which occurs when a control parameter, μ, reaches a critical value. The saddle-node is the prototypical example of B-tipping as it is the only generic bifurcation in one dimension for continuous dynamical systems [49]. Different systems with a saddle-node bifurcation all experience similar dynamics near a bifurcation [22] and therefore we choose as simple an equation of motion as possible, to which we add weak additive white noise of magnitude σ.

Mathematically, we take a system with state variable Φ evolving over time, t, with dynamics controlled by the stochastic differential equation

$$\frac{\mathrm{d}\Phi}{\mathrm{d}t} = \frac{1}{\epsilon} f(\Phi, \mu) + \frac{\sigma}{\sqrt{\epsilon}} \eta(t) \tag{1}$$

where the deterministic dynamics, f, are defined by

$$f(\Phi, \mu) = \Phi - \frac{1}{3}\Phi^3 - \mu \tag{2}$$

and η is white noise with mean and covariance

$$\langle \eta(t) \rangle = 0 \tag{3}$$

$$\langle \eta(t)\, \eta(t') \rangle = \delta(t - t'). \tag{4}$$

Due to its simplicity, this and closely related systems are commonly used in investigations of EWSs [29, 35, 50].

The timescale ratio ϵ controls the rate of adjustment in the system. A small ϵ gives a system that relaxes rapidly to equilibrium. For $\mu = 0$, equation (1) has an equilibrium with $\Phi^* = \sqrt{3}$. If μ is increased from zero, then Φ^* decreases. Eventually, the critical value of $\mu_c = 2/3$ is reached, (with corresponding equilibrium $\Phi^* = 1$), at which point the system undergoes a saddle-node bifurcation.

It is often useful to write the dynamics of equation (1), $f(\Phi, \mu)$, as the derivative of a potential function, $V(\Phi, \mu)$. Writing equation (1) in this way gives

$$\frac{\mathrm{d}\Phi}{\mathrm{d}t} = -\frac{1}{\epsilon}\frac{\mathrm{d}V}{\mathrm{d}\Phi} + \frac{\sigma}{\sqrt{\epsilon}} \eta(t) \tag{5}$$

where

$$V(\Phi) = -\frac{1}{2}\Phi^2 + \frac{1}{12}\Phi^4 + \mu\Phi. \tag{6}$$

This has the interpretation that the dynamics of the system minimise V and that the minima of V correspond to different equilibria. As the tipping point approaches, the minimum the system is in will become broader and shallower. Once the tipping point is reached, the minimum will no longer exist and the system will transition to a new minimum.

2.1.2. With spatial interactions

To take into account the spatial nature of the problem we must allow for spatial dynamics. For simplicity, we restrict ourselves to a one dimensional periodic domain of length $L = 2\pi$. We parameterise spatial interactions by adding a diffusive coupling to equation (1); this acts to smooth out the value of Φ over the domain. Such a parameterisation has found numerous uses in climate and ecological models. For example, it has been used in energy balance models for the global temperature [51, 52], ecosystem pattern formation [53, 54] and accounting for spatial effects in models of tipping phenomena [55, 56].

We use the equation

$$\frac{\partial \Phi}{\partial t} = \frac{1}{\epsilon}\left(f(\Phi,\mu) + D\frac{\partial^2 \Phi}{\partial x^2}\right) + \sigma\sqrt{\frac{L}{\epsilon}}\zeta(x,t), \tag{7}$$

where the strength of the spatial interactions are quantified by the diffusion coefficient, D. The field ζ is white noise, in both time and space, with zero mean and covariance

$$\langle \zeta(x,t)\,\zeta(x',t')\rangle = \delta(t-t')\,\delta(x-x'). \tag{8}$$

We scale the noise term by the square root of the domain size, L, to ensure that the spatial average of the noise term is equal in magnitude to the noise term in equation (1) (see appendix A). Equation (1) can thus be considered a mean field approximation of equation (7).

Equation (7) is a time-dependent Ginzburg–Landau equation which has been used in the study of Ising ferromagnets [57]. Like equation (1), it can also be understood as the derivative of a potential. However, as the state of the system is no longer given by a number but instead by a field, $\Phi(x)$, the potential function, $V(\Phi)$, must be replaced with a functional, $\mathcal{V}[\Phi(x)]$, and the derivative by a functional derivative. Writing equation (7) in this way gives

$$\frac{\partial \Phi}{\partial t} = -\frac{1}{\epsilon}\frac{\delta \mathcal{V}}{\delta \Phi} + \sigma\sqrt{\frac{L}{\epsilon}}\zeta(x,t) \tag{9}$$

where

$$\mathcal{V}[\Phi(x)] = \int_0^L V(\Phi(x,\mu)) + \frac{D}{2}\left(\frac{\partial \Phi}{\partial x}\right)^2 \mathrm{d}x. \tag{10}$$

When written in this form, the close analogy between equations (9) and (5) becomes clear. Even in the spatially extended case, the system still acts to minimise a potential, $\mathcal{V}$. Again, different minima of $\mathcal{V}$ correspond to different equilibria of the system. As the tipping point approaches, $\mathcal{V}$ becomes broader and shallower, until the minimum disappears at the tipping point. After this the system as a whole transitions to a new equilibrium.

This way of writing the equation also makes clear that any equilibrium of equation (7) must be spatially uniform. This is because equation (10) depends on the square of the spatial gradient of Φ, and is this minimised when Φ is uniform.

2.2. Early warning indicators (EWIs)

2.2.1. Temporal early warning

We begin by showing how the commonly used EWIs of variance and autocorrelation arise. We study the dynamics of fluctuations about equilibrium. To that end, we linearise equation (1) about an equilibrium given implicitly by $f(\Phi^*,\mu) = 0$ and set $\phi = \Phi - \Phi^*$. This gives

$$\frac{\mathrm{d}\phi}{\mathrm{d}t} = -\frac{\lambda}{\epsilon}\phi + \frac{\sigma}{\sqrt{\epsilon}}\eta(t), \tag{11}$$

where $\lambda = -\partial_\Phi f(\Phi^*,\mu)$.

With this sign convention λ decreases towards zero as the system approaches the tipping point. As fluctuations return to equilibrium on a timescale of ϵ/λ, this timescale diverges as the tipping point is reached; this is known as *critical slowing down*. Detecting this timescale divergence would therefore give an early warning of tipping.

Equation (11) is known as an Ornstein–Uhlenbeck process [58]. This equation has known variance and lag-T autocorrelation, given by

$$\mathrm{Var}\,\phi = \frac{\sigma^2}{2\lambda} \tag{12}$$

$$A_T(\phi) = \mathrm{e}^{-\lambda T/\epsilon}. \tag{13}$$

Both of these quantities depend on the system timescale and can thus give an early warning of tipping. As the tipping point is approached, the variance diverges and the autocorrelation tends to unity.

These EWSs can also be understood using the framework of the potential function, V. The equilibrium of the system corresponds to a minimum of V about which there will be small fluctuations due to noise. The magnitude of these fluctuations will be controlled by the curvature of the potential as $V''(\Phi^*) = \lambda$. As the tipping point approaches, $V''(\Phi^*)$ decreases and the minimum broadens. As a result the fluctuations become larger and longer lived, leading to increases in variance and autocorrelation.

2.2.2. Spatial early warning

We now show that critical slowing down will still occur in the presence of spatial interactions. Again, we linearise equation (7) about a spatially uniform equilibrium given implicitly by the conditions $f(\Phi^*(x), \mu) = 0$ and $\partial_x \Phi^* = 0$. We set $\phi(x) = \Phi(x) - \Phi^*(x)$ and linearise to get

$$\frac{\partial \phi}{\partial t} = -\frac{\lambda}{\epsilon}\phi + \frac{D}{\epsilon}\frac{\partial^2 \phi}{\partial x^2} + \sigma\sqrt{\frac{L}{\epsilon}}\zeta(x,t), \tag{14}$$

where $\lambda = -\partial_\Phi f(\Phi^*, \mu)$.

It is easiest to see the effects of critical slowing down by decomposing $\phi(x)$ into a Fourier series. The coefficients, $F_k(t)$, of the Fourier series of a function $F(x,t)$ relate to F through

$$F(x,t) = \frac{1}{L}\sum_{k=-\infty}^{\infty} F_k(t)\,\mathrm{e}^{\mathrm{i}kx}, \tag{15}$$

and can be explicitly calculated using

$$F_k(t) = \int_0^L F(x,t)\,\mathrm{e}^{-\mathrm{i}kx}\mathrm{d}x. \tag{16}$$

With these definitions applied to $\phi(x,t)$ and $\zeta(x,t)$, the dynamics for each mode, k, in equation (14) decouple and become

$$\frac{\mathrm{d}\phi_k}{\mathrm{d}t} = -\frac{\lambda}{\epsilon}\left(1 + \xi^2 L^2 k^2\right)\phi_k + \sigma\sqrt{\frac{L}{\epsilon}}\zeta_k(t) \tag{17}$$

where

$$\xi = \frac{1}{L}\sqrt{\frac{D}{\lambda}}. \tag{18}$$

Appendix B shows that ξ can be understood as the correlation length of the system, normalised by the domain size.

Equation (17) shows that each mode relaxes to equilibrium over a timescale

$$\tau_k = \frac{\epsilon}{\lambda}\frac{1}{(1 + \xi^2 L^2 k^2)}. \tag{19}$$

Therefore as the bifurcation is approached and λ reduces towards zero, the timescale of each mode increases. This is another example of critical slowing down. In particular the timescale of the spatial mean fluctuation, which corresponds to $k = 0$, diverges.

This timescale increase occurs if there is no spatial coupling ($D = 0$) and if there is spatial coupling ($D \neq 0$). Any method that can detect this increase, such as measuring the variance and autocorrelation, can therefore give an early warning. We may expect this to be most easy to detect when D is small, as in this case the system behaves approximately like an ensemble of independent tipping systems, each of which experiences a rise in variance and autocorrelation before the tipping point.

Again, this can be understood using the potential framework. As the tipping point is approached, $\mathcal{V}$ will broaden. This means that the fluctuations, $\phi(x)$, will be larger and longer lived. As $\phi(x)$ is a field, the fluctuations correspond to changes in space and thus we should expect increases in spatial variance and autocorrelation.

Table 2. Parameter values assumed in this study.

Parameter	Value range
ϵ	10^{-3} to 10^{1}
D	0 to 10^{3}
σ	0.03
L	2π

2.2.3. Correlation length

Although we have introduced a parameter, D, to quantify the magnitude of spatial coupling, we performed the analysis of section 2.2.2 in terms of the normalised correlation length, ξ. To help our results generalise to other functional forms for spatial coupling we will continue to use ξ rather than D. This is because D is specific to our model system but a correlation length will exist for a range of other couplings. There are some additional advantages to working with ξ over D. For example, it is straightforward to estimate ξ directly from data, by measuring how rapidly correlations decay in space. Additionally, we will see that our results about the skill of spatial EWSs are best understood in terms of ξ rather than D.

It should be noted, that at the bifurcation the value of λ is zero, which means that ξ diverges. This can be used as an early warning signal in its own right. However, we do not examine that phenomenon directly in this study. Instead, we will calculate the correlation length for the initial state of the system with $\mu = 0$.

2.3. Experimental configuration

We perform experiments by increasing μ from zero linearly with time, with $\dot{\mu} = 1$, and numerically integrating the model. As the system has a timescale on the order of ϵ^{-1}, this corresponds to a slow parameter change when $\epsilon \ll 1$ and a rapid change when $\epsilon \gg 1$. We perform experiments with both equation (1) (without spatial dynamics) and equation (7) (with spatial dynamics). We can also perform control simulations in which the system does not tip by keeping μ fixed at zero.

We initialise Φ in equation (1) with a random variable drawn from a normal distribution of mean $\sqrt{3}$ and variance equal to the exact variance of the linearised system. Similarly, we initialise equation (7) with a random field with a spatially uniform mean of $\sqrt{3}$ and covariance given by the exact covariance of the linearised system equation (14). This ensures that on average the system is initialised in equilibrium and changes in variance and autocorrelation are due to stability changes rather than the system spinning up.

We numerically integrate the system forward in time from $t = 0$ to $t = 0.6$, using parameter values given in table 2. This means the system does not reach the tipping point (which occurs at $t = 2/3$). As the probability of N-tipping increases as the system approaches the tipping point, stopping the integration before the tipping point minimises the effect of N-tipping on our results. For the same reason, we set σ to be small.

We integrate equations (1) and (7) with an implicit Runge–Kutta method. We carry this out numerically with the diffrax library [59]. The solver uses an internal time step of 0.0001 and we sample output after $\Delta t = 0.001$ units of time. We discretise equation (7) into $N = 10$ points in space and approximate the second derivative with central finite differences.

2.3.1. Temporal EWIs

To produce temporal EWIs we analyse each time series in a sliding window over the data. We express the window length as a window fraction which we define as the ratio of the window size to the total duration of the series. Within each window we detrend by fitting and subtracting a cubic polynomial, and we then compute the variance and the autocorrelation (at lag Δt) from the residuals.

2.3.2. Spatial EWIs

Spatial EWIs differ in that they are computed instantaneously from the data and therefore do not require a sliding window. For similar reasons, no detrending is required.

For a field $q(x, t)$, we define the spatial mean at time t as

$$\overline{q} = \frac{1}{L}\int_0^L q(x,t)\,\mathrm{d}x. \tag{20}$$

This allows us to write the spatial variance of q as

$$V_s(q) = \overline{q^2} - \overline{q}^2 \tag{21}$$

and the spatial autocorrelation at lag T, which we take as Δt throughout the paper,

$$A_{s,T}(q) = \frac{\overline{q'(x,t)\,q'(x,t+T)}}{\sqrt{V_s(q(x,t))\,V_s(q(x,t+T))}} \tag{22}$$

where

$$q' = q - \overline{q}. \tag{23}$$

2.4. Quantifying skill

An increase in the EWIs of variance and autocorrelation is evidence that a system is approaching a tipping point. As such trends may arise due to random variability, we measure the significance of the trend using the surrogate phase method [60]. We generate 1000 phase randomised surrogates of the EWI and compute the linear trend for each surrogate. In general we expect a nonlinear increase in the EWI before the bifurcation, however we measure a linear trend as it is difficult to determine *a priori* what the nonlinear trend should be. We deem an observed linear trend as significant at level p if it exceeds a fraction $1-p$ of the surrogate trends.

Classifying EWSs in this manner allows us to quantify their skill at predicting approaching tipping points using ROC analysis [61]. For a given significance level p, we generate 5000 time series of the EWI for the system with increasing μ and compute how many significant trends are observed, giving the true positive rate. We repeat this for the control simulation (μ held constant) to give the false positive rate.

Plotting the true positive rate against the false positive rate gives the ROC curve. The overall skill of the EWS is summarised by the area under that curve (AUC). By construction, the AUC is bounded between 0 and 1. A maximally skilful early warning signal will have an AUC of 1, whereas an early warning signal with no skill at all will have an AUC of 1/2. If the AUC is smaller than this, the EWS is worse than random chance.

2.5. False positives

Some studies have demonstrated how EWSs can still give an indication of an approaching tipping point even in cases where no such tipping point exists [62, 63]. To investigate this, we perform experiments in which the system moves away from the bifurcation point, by setting $\dot{\mu} = -1$ and performing the numerical procedure outlined in section 2.3.

For each generated time series, we compute EWIs and evaluate their significance as described in section 2.4. Since the system cannot tip, any significant increase represents a false positive. A trend is taken to give an early warning of tipping if $p < 0.05$. Therefore, the false positive rate is the proportion of trends satisfying this criterion.

3. Results

3.1. Temporal EWIs

We measure how the skill of temporal EWIs depend on the system timescale. As temporal EWIs require a sliding window, we investigate how the skill is affected by the length of this window. We perform the experiment given in section 2.3 using the model without spatial dynamics, equation (1), and quantify their skill with the AUC, as described in section 2.4. This was carried out for a range of ϵ values between 10^{-3} and 10 and window lengths with sizes between 1% and 99% of the time series length. We plot the resulting AUC in figure 1.

Figure 1 shows that when the timescale of the system is slow compared to the forcing timescale (large ϵ), temporal EWIs show little skill. However, when the timescale of the system is much faster than the forcing timescale, skilful early warnings can be obtained.

If the window size is chosen optimally, then the early warning indicators show skill for ϵ values smaller than around 10^{-1}. However, if the choice is made sub-optimally this can fall to below 10^{-2}. For small values of ϵ, temporal early warning signals are skilful for a range of window sizes, as long as they are not too long or too short.

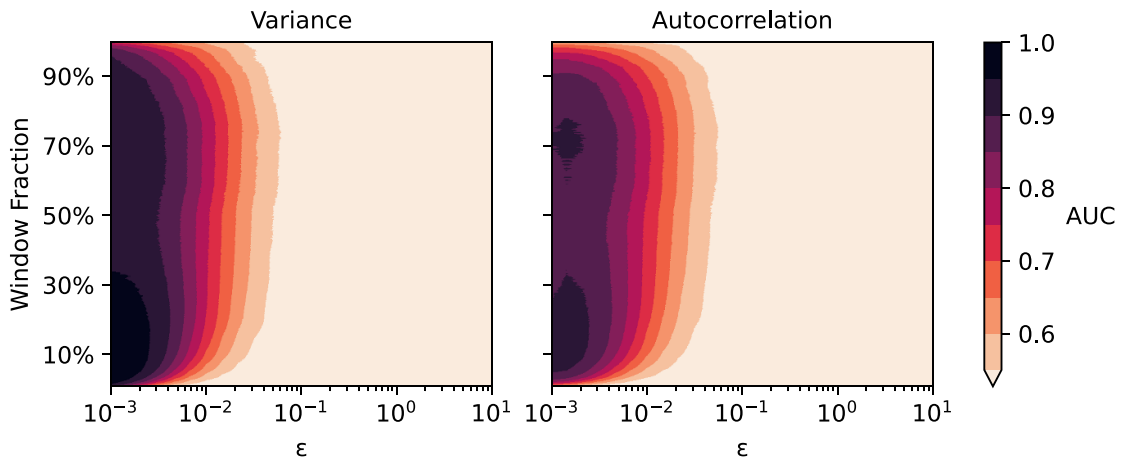

Figure 1. Early warning signal skill, quantified by the AUC, for the temporal early warning indicators of variance and autocorrelation. Both early warning signals are skilful for similar values of ϵ, as long as ϵ is smaller than around 10^{-1}. The skill is relatively insensitive to the choice of sliding window length as long as it is not very short or very long.

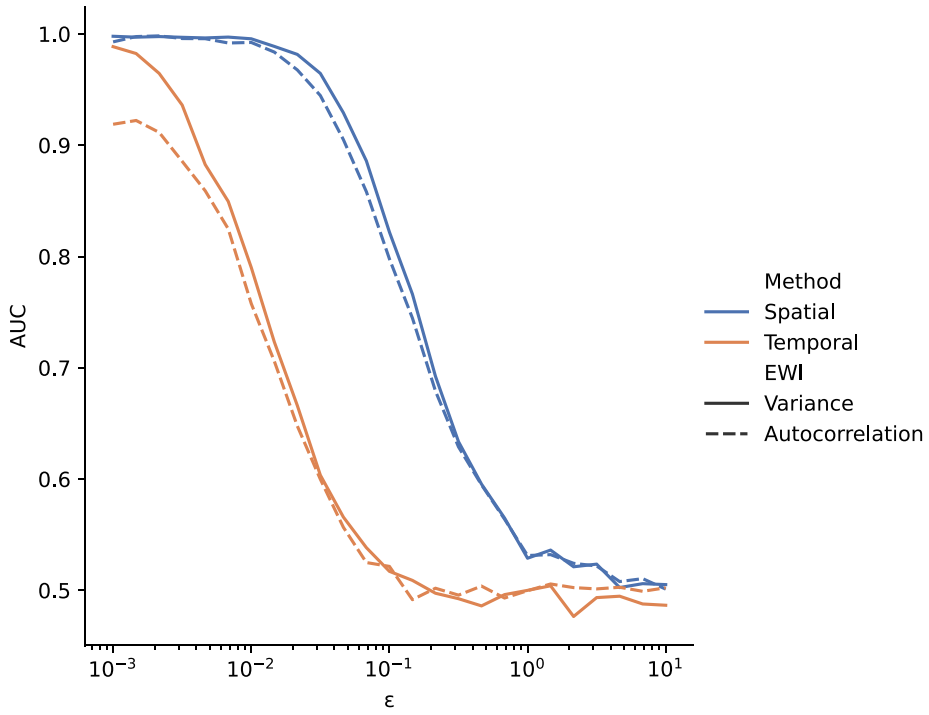

Figure 2. A comparison of the skill of spatial (blue) and temporal (orange) early warning signals as a function of ϵ assuming no spatial coupling. Spatial early warning signals are more skilful over the range of ϵ considered, and remain skilful for larger ϵ than temporal early warning signals. In particular, there is still some skill as ϵ approaches 1.

3.2. Spatial early warning

3.2.1. Uncoupled limit

First, we consider the limiting case of zero correlation length (which corresponds to $D = 0$). In this case, ensemble averages and spatial averages are equivalent, and so we expect to get good early warning signals.

We calculate the skill of spatial EWSs for the system with spatial dynamics (equation (7)) for a range of ϵ values. We compare this to the skill of temporal EWSs applied to the spatial mean of the system, $\overline{\Phi}$. When calculating the temporal EWIs, we use the optimal window length for each ϵ, which is the window length with highest skill for a given ϵ in figure 1.

The results of this experiment are plotted in figure 2. The figure shows that spatial EWSs are more skilful than temporal early warning signals, when $\xi = 0$, across all ϵ values. Furthermore, spatial EWSs

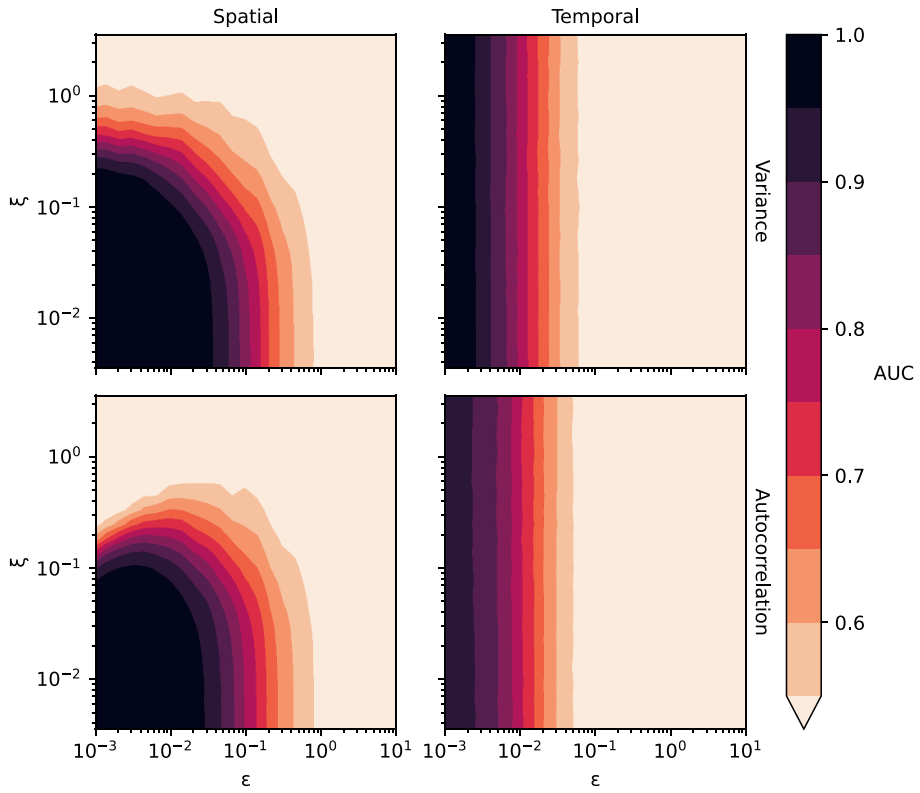

Figure 3. The skill of spatial and temporal early warning signals as a function of ϵ and normalised correlation length. Spatial early warning indicators are more skilful at larger values of ϵ but temporal ones are more skilful as ξ increases.

retain some skill for $\epsilon \approx 1$, whereas temporal EWSs are only skilful for ϵ smaller than 10^{-1}. This represents an order of magnitude improvement of spatial EWSs over their temporal equivalent in the uncoupled regime.

3.2.2. Role of spatial correlations

We now continue the experiment of section 3.2.1 for the case where $\xi \neq 0$. That is, we calculate spatial early warning indicators over the whole domain and also calculate temporal early warning indicators of the system's spatial mean. Again, temporal indicators require a choice of sliding window, which we set for each ϵ to be the window length that gives the most skilful early warning as identified in figure 1. The results of varying ξ (through varying D) and ϵ are shown in figure 3. Figure 3 shows that temporal EWIs, calculated with optimal window lengths, are skilful for any ξ value as long as the corresponding ϵ value is small enough. The skill of the temporal early warning indicators do not vary with ξ. The critical ϵ, above which temporal EWIs show no skill, is around 10^{-1}.

Conversely, spatial EWIs show no skill when ξ is too large. This loss of skill happens for normalised correlation lengths above $\xi \approx 1$. This can be readily understood as having a correlation length similar to the domain size, meaning there are no effectively independent parts of the domain. However, spatial EWIs are more skilful than temporal early warning indicators for systems with slow timescales (large ϵ). They show some skill even for $\epsilon \approx 1$, representing an order of magnitude improvement.

It is interesting to note that the autocorrelation appears to lose some skill at small ϵ compared to the variance in the spatial case. This is a result of having a fixed time step. As ϵ gets smaller, the system changes less from one time step to the next, so it becomes more challenging to estimate the autocorrelation. This could be alleviated by calculating the autocorrelation over a longer time step.

The most skilful method of early warning, either spatial or temporal, is plotted in figure 4. Where neither method is skilful (i.e. neither method has an AUC above 0.5) the figure is left blank. It shows a summary of the results, namely if ϵ is larger and ξ not too big then spatial early warning indicators are most suitable. However if ξ is large and ϵ small then temporal EWIs are better. However in the domain of very large ϵ, neither method can give skilful early warning signals.

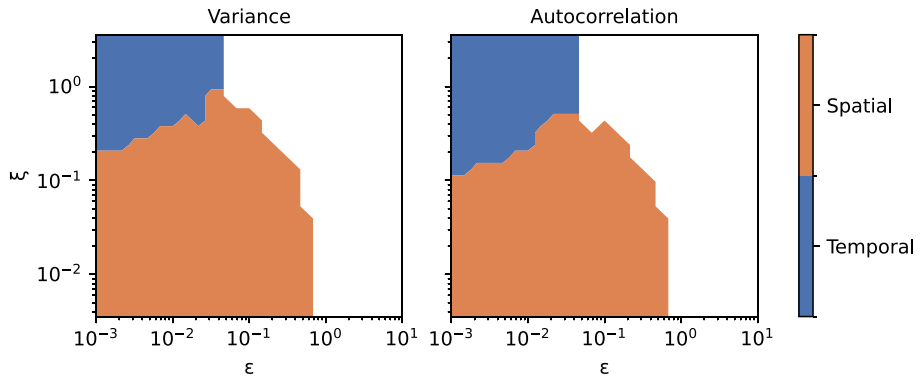

Figure 4. This figures shows which of spatial and temporal early warning signals are more skilful as a function of ϵ and ξ. Where neither spatial or temporal early warning signals are skilful the plot is left blank.

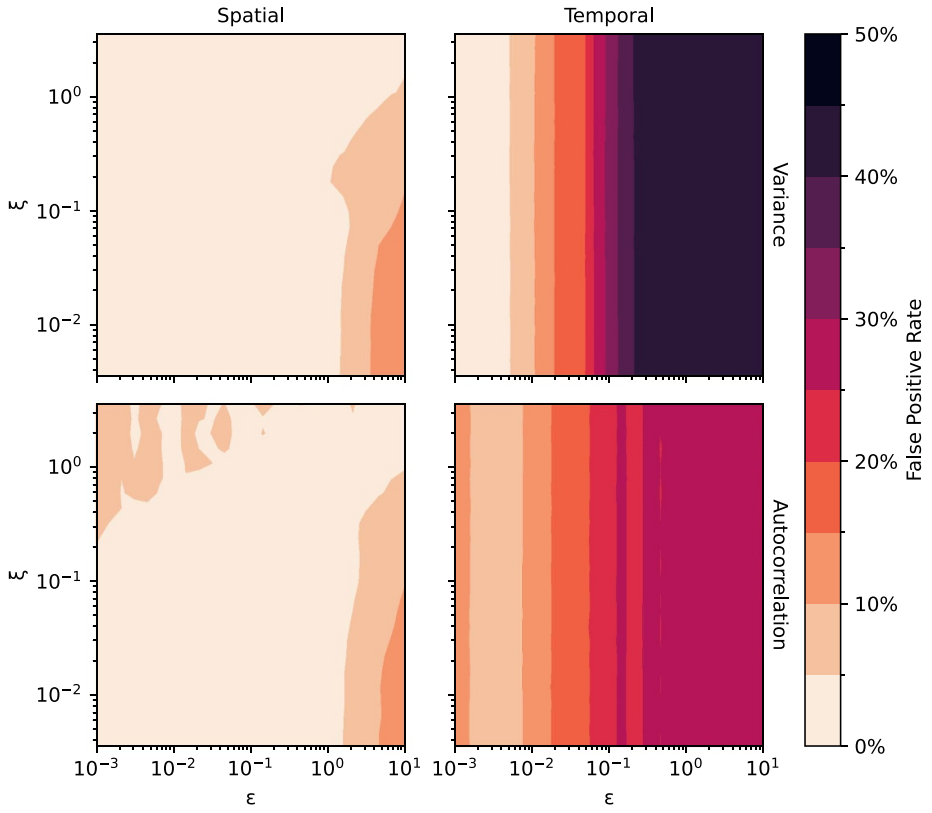

Figure 5. The false positive rate for the case where μ varies in time but the system does not approach a bifurcation. Spatial early warning signals outperform their temporal counterparts, particularly at large ϵ.

3.2.3. False positives

As described in section 2.5, we compare how spatial and temporal EWIs differ in their probability of producing spurious trends by calculating the false positive rate when $\dot{\mu} = -1$. The window lengths used to calculate the temporal EWIs were chosen similarly to how they were chosen to calculate the AUC. Namely, they were the window lengths which minimised the false positive rate in the uncoupled system.

We calculate the false positive rate for spatial and temporal variance and autocorrelation across a range of ϵ and ξ values, which we plot in figure 5. We find that for the parameters considered, spatial EWIs generate fewer false positives than their temporal counterparts. This difference is particularly pronounced at large ϵ.

4. Discussion

There is substantial evidence that the Earth system contains subsystems in which climate change could cause tipping from one state to another, leading to profound impacts on society. As there is little consensus amongst ESMs on the level of climate change required for tipping, it is important to develop EWIs. Although progress has been made on temporal indicators [23], temporal EWIs struggle with three issues in particular.

Firstly, Earth system tipping elements are being forced rapidly compared to their intrinsic timescales, as shown in table 1. Secondly, remote sensing [64] provides data with a high spatial resolution, which temporal indicators do not use. Thirdly, the time series of observables of a tipping element are relatively short [65], especially when compared to their intrinsic timescales. We have developed an approach which can begin to address these issues by using spatial information.

In this paper, we have compared the skill of temporal and spatial EWSs for tipping points. We used a simple reaction-diffusion system with a saddle node bifurcation. We could control how rapidly the system was forced compared to its own intrinsic timescale by adjusting the parameter ϵ. We could also change the how strong the spatial interactions were, which we quantified with a correlation length, ξ.

We found that spatial and temporal EWIs have their own strengths and weaknesses. We find that for systems that are forced rapidly relative to their timescale (larger ϵ), spatial early warning signals may be skilful but temporal early warnings are not. However, when there are strong spatial correlations (correlation lengths on the order of the domain size), spatial early warnings are not skilful. Conversely, when the forcing is slow, temporal early warning signals can be skilful no matter the spatial correlation.

We found that the correlation length of the system was an important factor in controlling the skill of spatial EWSs. For systems like forest ecosystems, which have a relatively short correlation length [66] we may expect spatial EWIs to be skilful. However, for systems that are more spatially coherent like ocean circulations [17], spatial EWSs may be less skilful than temporal ones. Furthermore, systems which are rapidly forced and strongly spatially coherent are not amenable to skilful temporal or spatial early warnings. A system specific approach may be required in this case.

These results are important for Earth system tipping elements with larger ϵ values. These systems have significant inertia and allow for a temporary overshoot of their tipping point [67, 68], which is a reason why it is important to understand how close the tipping point is. As well as making use of the spatial information provided by remote sensing data, spatial early warning indicators do not need to be calculated from long time series. This is because they can give an instantaneous measure of the system's stability and do not require detrending over a sliding window.

A limitation of our study is that we only investigated a simple one dimensional scalar field subject to additive white noise. Furthermore, we modelled spatial interactions with a diffusive spatial coupling. It is possible that a more complicated coupling could affect our results. For example, we found that the skill of temporal early warning signals are independent of ξ, which may be due to the fact that the diffusion term vanishes in the spatial mean. Furthermore, we assumed the system and the forcing was homogeneous in space. This assumption will not hold, for example, in systems with a strong latitudinal gradient.

For systems that are heterogeneous in space, care will be needed when trying to detect spatial EWSs. As the early warning signals studied here are caused by changes in the statistics of the system's fluctuations about equilibrium, a non-uniform spatial equilibrium may need to be subtracted from the data to isolate the fluctuations in this case. Similarly, if the change in the forcing is not spatially uniform, we may expect changes in the variability of the system for reasons that are unrelated to its stability. Nevertheless, we conjecture that spatial EWSs can still be skilful in a range of systems as long as they are analysed on scales large compared with the correlation length of the fluctuations and small compared with the length scale of the forcing.

In summary, we have demonstrated a complementarity between spatial and temporal EWIs. We found spatial early warnings to be more skilful when the forcing is rapid and the spatial coupling weak, but temporal signals to be more skilful when the forcing is slow and the spatial coupling strong. Understanding when which technique is most appropriate will enable a more effective use of early warning indicators.

Acknowledgments

P D L R and P C acknowledge support from the European Union's Horizon Europe research and innovation programme under Grant Agreement No. 101137601 (ClimTip): Funded by the European Union. P D L R, P C and C H acknowledge support from the UK Advanced Research and Invention Agency

(ARIA) via the project 'AdvanTip'. J C, C H and P C acknowledge support from the PREDICT project which has received funding from the European Space Agency (ESA) under ESA Contract No. 4000146344/24/I-LR.

Data availability statement

The data that support the findings of this study are openly available at the following URL/DOI: www.github.com/josephjclarke/spatial_temporal_early_warning_skill [69].

Author contributions

J C: Formal Analysis, Methodology, Investigation, Visualisation, Writing, C H: Methodology, Writing P D L R: Methodology, Writing, P C: Conceptualisation, Supervision, Writing.

Appendix A. Spatio-temporal white noise

If $\zeta(x,t)$ is spatio-temporal white noise, then

$$\langle \zeta(x,t) \rangle = 0 \tag{24}$$

$$\langle \zeta(x,t)\,\zeta(x',t') \rangle = \delta(x-x')\,\delta(t-t'). \tag{25}$$

Now we show $\overline{\sqrt{L}\zeta(x,t)}$ is temporal white noise with the classic correlation structure. The mean is

$$\left\langle \overline{\sqrt{L}\zeta(x,t)} \right\rangle = \left\langle \frac{\sqrt{L}}{L}\int_0^L \zeta(x,t)\,\mathrm{d}x \right\rangle \tag{26}$$

$$= \frac{1}{\sqrt{L}}\int_0^L \langle \zeta(x,t) \rangle \mathrm{d}x \tag{27}$$

$$= 0 \tag{28}$$

and the covariance

$$\left\langle \overline{\sqrt{L}\zeta(x,t)}\,\overline{\sqrt{L}\zeta(x',t')} \right\rangle = \left\langle \frac{\sqrt{L}}{L}\int_0^L \zeta(x,t)\,\mathrm{d}x \frac{\sqrt{L}}{L}\int_0^L \zeta(x',t')\,\mathrm{d}x' \right\rangle \tag{29}$$

$$= \left\langle \frac{1}{L}\int_0^L\int_0^L \zeta(x,t)\,\zeta(x',t')\,\mathrm{d}x\mathrm{d}x' \right\rangle \tag{30}$$

$$= \frac{1}{L}\int_0^L\int_0^L \langle \zeta(x,t)\,\zeta(x',t') \rangle \mathrm{d}x\mathrm{d}x' \tag{31}$$

$$= \frac{1}{L}\int_0^L\int_0^L \delta(x-x')\,\delta(t-t')\,\mathrm{d}x\mathrm{d}x' \tag{32}$$

$$= \delta(t-t'). \tag{33}$$

Appendix B. Correlation length

We calculate the correlation length by linearising equation (7) to give

$$\frac{\partial \phi}{\partial t} = \frac{1}{\epsilon}\left(D\frac{\partial^2 \phi}{\partial x^2} - \lambda\phi\right) + \sigma\sqrt{\frac{L}{\epsilon}}\zeta(x,t), \tag{34}$$

and calculating the associated Green's function, given by the solution to

$$\frac{\partial G}{\partial t} = \frac{1}{\epsilon}\left(D\frac{\partial^2}{\partial x^2} - \lambda\right) G(x,t) + \delta(t)\,\delta(x). \tag{35}$$

This Green's function controls the response to fluctuations, so its dependence on x will reveal the correlation length. It is easiest to solve equation (35) by using Fourier methods. For simplicity, we take the limit as $L \to \infty$ so that the Fourier transform of $G(x,t)$ is given by

$$\widetilde{G}(k,\omega) = \frac{1}{4\pi^2} \iint G(x,t) \exp\left(i(kx+\omega t)\right) \mathrm{d}x\mathrm{d}t \tag{36}$$

and the inverse transform is

$$G(x,t) = \iint \widetilde{G}(k,\omega) \exp\left(-i(kx+\omega t)\right) \mathrm{d}k\mathrm{d}\omega. \tag{37}$$

After applying this transform, equation (35) becomes

$$i\omega\widetilde{G} = -\frac{1}{\epsilon}\left(Dk^2+\lambda\right)\widetilde{G}+1 \tag{38}$$

or

$$\widetilde{G} = \frac{1}{\lambda}\frac{1}{\epsilon^{-1}+\epsilon^{-1}k^2\xi^2+i\omega\lambda^{-1}}, \tag{39}$$

with $\xi^2 = D/\lambda$. $\widetilde{G}$ can be inverted to give

$$G(x,t) = \frac{1}{\xi}\frac{\epsilon}{\sqrt{4\pi\lambda t}} \exp\left(-\frac{1}{4}\frac{x^2}{\xi^2}\frac{\epsilon^2}{\lambda t}\right) \mathrm{e}^{\frac{-\lambda t}{\epsilon}}. \tag{40}$$

This justifies that ξ is a correlation length as when $x \gg \xi$ we have $G \approx 0$.

ORCID iDs

Joseph Clarke 0000-0002-6250-1543
Chris Huntingford 0000-0002-5941-7770
Paul D L Ritchie 0000-0002-7649-2991
Peter Cox 0000-0002-0679-2219

References

[1] Lenton T M, Held H, Kriegler E, Hall J W, Lucht W, Rahmstorf S and Schellnhuber H J 2008 Tipping elements in the Earth's climate system *Proc. Natl Acad. Sci.* **105** 1786–93
[2] Drijfhout S, Bathiany S, Beaulieu C, Brovkin V, Claussen M, Huntingford C, Scheffer M, Sgubin G and Swingedouw D 2015 Catalogue of abrupt shifts in Intergovernmental Panel on Climate Change climate models *Proc. Natl Acad. Sci.* **112** E5777–86
[3] Angevaare J R and Drijfhout S S 2025 Catalogue of strong nonlinear surprises in ocean, sea-ice, and atmospheric variables in CMIP6 (available at: https://egusphere.copernicus.org/preprints/2025/egusphere-2025-2039/)
[4] Stommel H 1961 Thermohaline convection with two stable regimes of flow *Tellus* **13** 224–30
[5] Rahmstorf S 1995 Bifurcations of the Atlantic thermohaline circulation in response to changes in the hydrological cycle *Nature* **378** 145–9
[6] Drijfhout S, Angevaare J R, Mecking J, Van Westen R M and Rahmstorf S 2025 Shutdown of northern Atlantic overturning after 2100 following deep mixing collapse in CMIP6 projections *Environ. Res. Lett.* **20** 094062
[7] Cox P M, Betts R A, Jones C D, Spall S A and Totterdell I J 2000 Acceleration of global warming due to carbon-cycle feedbacks in a coupled climate model *Nature* **408** 184–7
[8] Hirota M, Holmgren M, Van Nes E H and Scheffer M 2020 Global resilience of tropical forest and savanna to critical transitions *Science* **334** 232–5
[9] Garbe J, Albrecht T, Levermann A, Donges J F and Winkelmann R 2020 The hysteresis of the Antarctic ice sheet *Nature* **585** 538–44
[10] Bochow N, Poltronieri A, Robinson A, Montoya M, Rypdal M and Boers N 2023 Overshooting the critical threshold for the Greenland ice sheet *Nature* **622** 528–36
[11] Gregory J M, Huybrechts P and Raper S C B 2004 Threatened loss of the Greenland ice-sheet *Nature* **428** 616–616
[12] Jackson L C, Kahana R, Graham T, Ringer M A, Woollings T, Mecking J V and Wood R A 2015 Global and European climate impacts of a slowdown of the AMOC in a high resolution GCM *Clim. Dyn.* **45** 3299–316
[13] Ritchie P D L *et al* 2020 Shifts in national land use and food production in Great Britain after a climate tipping point *Nat. Food* **1** 76–83
[14] Flores B M *et al* 2024 Critical transitions in the Amazon forest system *Nature* **626** 555–64
[15] Gatti L V *et al* 2021 Amazonia as a carbon source linked to deforestation and climate change *Nature* **595** 388–93
[16] Armstrong McKay D I, Staal A, Abrams J F, Winkelmann R, Sakschewski B, Loriani S, Fetzer I, Cornell S E, Rockström J and Lenton T M 2022 Exceeding 1.5°C global warming could trigger multiple climate tipping points *Science* **377** 6611
[17] Wood R A, Rodríguez J M, Smith R S, Jackson L C and Hawkins E 2019 Observable, low-order dynamical controls on thresholds of the Atlantic meridional overturning circulation *Clim. Dyn.* **53** 6815–34

[18] Parry I, Ritchie P and Cox P 2022 Evidence of Amazon rainforest dieback in CMIP6 models *EGUsphere* **2022** 1–11
[19] van Westen R M and Dijkstra H A 2024 Persistent climate model biases in the Atlantic Ocean's freshwater transport *Ocean Sci.* **20** 549–67
[20] Lohmann J, Dijkstra H A, Jochum M, Lucarini V and Ditlevsen P D 2024 Multistability and intermediate tipping of the Atlantic Ocean circulation *Sci. Adv.* **10** eadi4253
[21] Ashwin P, Wieczorek S, Vitolo R and Cox P 2012 Tipping points in open systems: bifurcation, noise-induced and rate-dependent examples in the climate system *Phil. Trans. R. Soc. A* **370** 1166–84
[22] Guckenheimer J and Holmes P 1983 *Nonlinear Oscillations, Dynamical Systems and Bifurcations of Vector Fields* (*Applied Mathematical Sciences* vol 42) (Springer)
[23] Dakos V *et al* 2024 Tipping point detection and early warnings in climate, ecological and human systems *Earth Syst. Dyn.* **15** 1117–35
[24] Scheffer M *et al* 2012 Anticipating critical transitions *Science* **338** 344–8
[25] Scheffer M *et al* 2009 Early-warning signals for critical transitions *Nature* **461** 53–59
[26] Dakos V, Scheffer M, Van Nes E H, Brovkin V, Petoukhov V and Held H 2008 Slowing down as an early warning signal for abrupt climate change *Proc. Natl Acad. Sci. USA* **105** 14308–12
[27] Held H and Kleinen T 2004 Detection of climate system bifurcations by degenerate fingerprinting *Geophys. Res. Lett.* **31** 1–4
[28] Ditlevsen P and Ditlevsen S 2023 Warning of a forthcoming collapse of the Atlantic meridional overturning circulation *Nat. Commun.* **14** 4254
[29] Boers N 2021 Observation-based early-warning signals for a collapse of the Atlantic meridional overturning circulation *Nat. Clim. Change* **11** 680–8
[30] Boers N and Rypdal M 2021 Critical slowing down suggests that the western Greenland Ice Sheet is close to a tipping point *Proc. Natl Acad. Sci.* **118** 1–7
[31] Boulton C A, Lenton T M and Boers N 2022 Pronounced loss of Amazon rainforest resilience since the early 2000s *Nat. Clim. Change* **12** 271–8
[32] Lenton T M 2011 Early warning of climate tipping points *Nat. Clim. Change* **1** 201–9
[33] Ben-Yami M, Skiba V, Bathiany S and Boers N 2023 Uncertainties in critical slowing down indicators of observation-based fingerprints of the Atlantic overturning circulation *Nat. Commun.* **14** 8344
[34] Smith T, Zotta R-M, Boulton C A, Lenton T M, Dorigo W and Boers N 2023 Reliability of resilience estimation based on multi-instrument time series *Earth Syst. Dyn.* **14** 173–83
[35] Clarke J J, Huntingford C, Ritchie P D L and Cox P M 2023 Seeking more robust early warning signals for climate tipping points: the ratio of spectra method (ROSA) *Environ. Res. Lett.* **18** 035006
[36] Morr A, Boers N and Ashwin P 2024 Internal noise interference to warnings of tipping points in generic multidimensional dynamical systems *SIAM J. Appl. Dyn. Syst.* **23** 2793–806
[37] Thompson J M T and Sieber J 2011 Climate tipping as a noisy bifurcation: a predictive technique *IMA J. Appl. Math.* **76** 27–46
[38] Kuehn C 2011 A mathematical framework for critical transitions: bifurcations, fast-slow systems and stochastic dynamics *Physica D* **240** 1020–35
[39] van der Bolt B, van Nes E H and Scheffer M 2021 No warning for slow transitions *J. R. Soc. Interface* **18** rsif.2020.0935
[40] Rogelj J, Fransen T, Elzen M G J, Lamboll R D, Schumer C, Kuramochi T, Hans F, Mooldijk S and Portugal-Pereira J 2023 Credibility gap in net-zero climate targets leaves world at high risk *Science* **380** 1014–6
[41] Kéfi S *et al* 2014 Early warning signals of ecological transitions: methods for spatial patterns *PLoS One* **9** e92097
[42] Donangelo R, Fort H, Dakos V, Scheffer M and Van Nes E H 2010 Early warnings for catastrophic shifts in ecosystems: comparison between spatial and temporal indicators *Int. J. Bifur. Chaos* **20** 315–21
[43] Carpenter S R and Brock W A 2010 Early warnings of regime shifts in spatial dynamics using the discrete Fourier transform *Ecosphere* **1** art10
[44] Dakos V, Kéfi S, Rietkerk M, Egbert N H and Scheffer M 2011 Slowing down in spatially patterned ecosystems at the brink of collapse *Am. Nat.* **177** E153–66
[45] Guttal V and Jayaprakash C 2009 Spatial variance and spatial skewness: leading indicators of regime shifts in spatial ecological systems *Theor. Ecol.* **2** 3–12
[46] Tirabassi G and Masoller C 2023 Entropy-based early detection of critical transitions in spatial vegetation fields *Proc. Natl Acad. Sci.* **120** e2215667120
[47] Kéfi S, Rietkerk M, Alados C L, Pueyo Y, Papanastasis V P, ElAich A and Ruiter P C 2007 Spatial vegetation patterns and imminent desertification in Mediterranean arid ecosystems *Nature* **449** 213–7
[48] Eby S, Agrawal A, Majumder S, Dobson A P and Guttal V 2017 Alternative stable states and spatial indicators of critical slowing down along a spatial gradient in a savanna ecosystem *Glob. Ecol. Biogeogr.* **26** 638–49
[49] Thompson J M T, Stewart H B and Ueda Y 1994 Safe, explosive and dangerous bifurcations in dissipative dynamical systems *Phys. Rev. E* **49** 1019–27
[50] Ditlevsen P D and Johnsen S J 2010 Tipping points: early warning and wishful thinking *Geophys. Res. Lett.* **37** 19
[51] Ghil M 1976 Climate stability for a sellers-type model *J. Atmos. Sci.* **33** 3–20
[52] North G R, Cahalan R F and Coakley J A 1991 Energy balance climate models *Rev. Geophys.* **19** 91–121
[53] Gowda K, Riecke H and Silber M 2014 Transitions between patterned states in vegetation models for semiarid ecosystems *Phys. Rev. E* **89** 022701
[54] Bastiaansen R, Jaïbi O, Deblauwe V, Eppinga M B, Siteur K, Siero E, Mermoz S, Bouvet A, Doelman A and Rietkerk M 2018 Multistability of model and real dryland ecosystems through spatial self-organization *Proc. Natl Acad. Sci.* **115** 11256–61
[55] Clarke J, Huntingford C, Ritchie P and Cox P 2021 The compost bomb instability in the continuum limit *Eur. Phys. J. Spec. Top.* **230** 3335–41
[56] Rietkerk M, Bastiaansen R, Banerjee S, Koppel J, Baudena M and Doelman A 2021 Evasion of tipping in complex systems through spatial pattern formation *Science* **374** 6564
[57] Goldenfeld N 2018 *Lectures on Phase Transitions and the Renormalization Group* 1st edn (CRC Press)
[58] Jacobs K 2010 *Stochastic Processes for Physicists - Understanding Noisy Systems* (Cambridge University Press)
[59] Kidger P 2022 On neural differential equations (arXiv:2202.02435)
[60] Boettner C and Boers N 2022 Critical slowing down in dynamical systems driven by nonstationary correlated noise *Phys. Rev. Res.* **4** 013230

[61] Ashwin P, Bastiaansen R, Von Der Heydt A S and Ritchie P D L 2025 Early warning skill, extrapolation and tipping for accelerating cascades *Proc. R. Soc. A* **481** 20250405
[62] Wagner T J W and Eisenman I 2015 False alarms: how early warning signals falsely predict abrupt sea ice loss *Geophys. Res. Lett.* **42** 10,333–10,341
[63] Rietkerk M, Skiba V, Weinans E, Hébert R and Laepple T 2025 Ambiguity of early warning signals for climate tipping points *Nat. Clim. Change* **15** 479–88
[64] Lenton T M *et al* 2024 Remotely sensing potential climate change tipping points across scales *Nat. Commun.* **15** 343
[65] Smeed D A *et al* 2018 The North Atlantic Ocean is in a state of reduced overturning *Geophys. Res. Lett.* **45** 1527–33
[66] Espírito-Santo F D *et al* 2014 Size and frequency of natural forest disturbances and the Amazon forest carbon balance *Nat. Commun.* **5** 3434
[67] Ritchie P D L, Clarke J J, Cox P M and Huntingford C 2021 Overshooting tipping point thresholds in a changing climate *Nature* **592** 517–23
[68] Ritchie P D L, Huntingford C and Cox P M 2025 ESD ideas: climate tipping is not instantaneous - the duration of an overshoot matters *Earth Syst. Dyn.* **16** 1523–6
[69] Clarke J 2026 Code for Conditions for Skilful Spatial and Temporal Tipping Point Early Warning Signals *Spatial Temporal Early Warning Skill* (available at: www.github.com/josephjclarke/spatial_temporal_early_warning_skill)